Dynamics of Two Ferromagnetic Insulators Coupled by Superconducting Spin Current

Risto Ojajärvi,[1] F. S. Bergeret,[2,3] M. A. Silaev,[1,4] and Tero T. Heikkilä[1]
[1]Department of Physics and Nanoscience Center, University of Jyväskylä, P.O. Box 35 (YFL), FI-40014 University of Jyväskylä, Finland
[2]Centro de Física de Materiales (CFM-MPC), Centro Mixto CSIC-UPV/EHU, Manuel de Lardizabal 5, E-20018 San Sebastián, Spain
[3]Donostia International Physics Center (DIPC), Manuel de Lardizabal 4, E-20018 San Sebastián, Spain
[4]Computational Physics Laboratory, Physics Unit, Faculty of Engineering and Natural Sciences, Tampere University, P.O. Box 692, FI-33720 Tampere, Finland

(Received 26 July 2021; accepted 21 March 2022; published 20 April 2022)

A conventional superconductor sandwiched between two ferromagnets can maintain coherent equilibrium spin current. This spin supercurrent results from the rotation of odd-frequency spin correlations induced in the superconductor by the magnetic proximity effect. In the absence of intrinsic magnetization, the superconductor cannot maintain multiple rotations of the triplet component but instead provides a Josephson type weak link for the spin supercurrent. We determine the analog of the current-phase relation in various circumstances and show how it can be accessed in experiments on dynamic magnetization. In particular, concentrating on the magnetic hysteresis and the ferromagnetic resonance response, we show how the spin supercurrent affects the nonequilibrium dynamics of magnetization which depends on a competition between spin supercurrent mediated static exchange contribution and a dynamic spin pumping contribution. Depending on the outcome of this competition, a mode crossing in the system can either be an avoided crossing or mode locking.

DOI: 10.1103/PhysRevLett.128.167701

Superconductivity is characterized by a U(1) symmetry breaking complex order parameter and the dissipationless supercurrent proportional to its phase gradient. In the context of spin transport, analogous spin superfluidity has been discussed in various scenarios [1]. Recent work on coherent spin transport in multilayers containing ferromagnetic (F) and superconducting (SC) elements has opened the question of dissipationless spin transport in superconductors [2–4]. While there are notions of dissipationless or conserved spin currents in such systems [5,6], it has remained unclear in which sense such spin currents can be observed in experiments on dynamical magnetization. Here we clarify the situation by showing how spin supercurrents (SS) naturally arise in ferromagnetic resonance (FMR) experiments involving two or more magnets, how it is linked to the gradient of the direction of the triplet order parameter, and how it mediates magnetic interactions.

What distinguishes the superconducting currents from normal persistent ones [7–9] is their robustness against disorder and interactions and the large length scales on which they occur. In F/SC systems SS depends on the magnetic proximity effect and its range is set by the coherence length of the SC.

Here we study SS in possibly the simplest superconducting system in which it can exist, namely, a SC sandwiched between two ferromagnetic insulators (FI) with noncollinear magnetizations (Fig. 1). This system was considered already in the 1960s by de Gennes who showed that the SC mediates an antiferromagnetic interaction between the magnetic moments of the two FIs [10]. We demonstrate that this interaction can also be interpreted as an equilibrium spin current, and generalize it for a SC with a finite length and finite spin scattering. We consider the magnetization dynamics of two FIs coupled by spin pumping and SS, and show that spin supercurrents can lead to decreased or increased damping of the FMR modes of the trilayer, as compared to unhybridized modes in the normal (N) state.

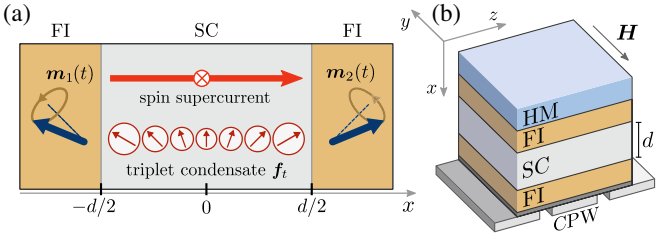

FIG. 1. (a) Spin supercurrent through a superconductor with thickness d. $\boldsymbol{m}_1(t)$ and $\boldsymbol{m}_2(t)$ are the instantaneous magnetization directions of the FIs, and the direction and radius of the "clocks" illustrate the spin direction and magnitude of the SC triplet condensate $\boldsymbol{f}_t$. (b) Sketch of an FMR experiment. The sample is mounted on a coplanar waveguide (CPW). The static field $\boldsymbol{H}$ is applied in the film plane. The additional heavy metal (HM) layer can be used to tune the Gilbert damping of the other FI.

Spin supercurrent in equilibrium.—We first illustrate the concept of SS with a scheme based on the linearized Usadel equation. Consider a SC of length d coupled with two noncollinear FIs, with magnetizations on $y-z$ plane pointing in directions $\boldsymbol{m}_1$ and $\boldsymbol{m}_2$ forming an angle ϕ. The effective exchange field at the SC/FI interface leads to a partial conversion of the conventional singlet superconducting condensate into a triplet component [11,12]. Thus, near T_c, the Matsubara Green's function (GF) for frequency $\omega_m > 0$ has the general form

$$\hat{g} = \tau_3 + (f_s + \boldsymbol{f}_t \cdot \boldsymbol{\sigma})\tau_1, \tag{1}$$

where f_s and $\boldsymbol{f}_t$ are the singlet and triplet condensate functions, respectively [13]. We assume translational invariance on the $y-z$ plane. The spin supercurrent in the x direction can then be expressed as [14]

$$\begin{aligned}\boldsymbol{j}_x^{\mathrm{eq}} &= \pi T \sum_{\omega_m>0} N_0 D \boldsymbol{f}_t \times \partial_x \boldsymbol{f}_t \\ &= \pi T \sum_{\omega_m>0} N_0 D |\boldsymbol{f}_t|^2 \partial_x \varphi \hat{\boldsymbol{x}},\end{aligned} \tag{2}$$

where φ is the angle of $\boldsymbol{f}_t$ relative to the z axis and N_0 is the density of states at the Fermi level in the normal state. The SS arises from the coherent rotation of the triplet Cooper pairs. The vector structure of $\boldsymbol{j}_x$ indicates its spin direction, and the subscript refers to the spatial direction.

The triplet condensate is determined by the Usadel equation and its boundary condition (BC)

$$D\nabla^2 \boldsymbol{f}_t = 2\omega_m \boldsymbol{f}_t, \tag{3a}$$

$$D\boldsymbol{n} \cdot \nabla \boldsymbol{f}_t|_{x=x_n} = 2iG_n \boldsymbol{m}_n f_s, \tag{3b}$$

where D is the diffusion constant, $\boldsymbol{n}$ is the interface normal from FI to SC, and $x_{1,2} = \mp d/2$. The interface parameters G_n, which are related to the imaginary spin mixing conductances of the interfaces by $\mathrm{Im}G_n^{\uparrow\downarrow} = G_n N_0$, determine the coupling between the singlet and triplet Cooper pairs [15,16]. To first order in G_n, the singlet retains its bulk value $f_s = \Delta/\omega_m$. The triplet condensate leads to a spin density [17,18]

$$\begin{aligned}\boldsymbol{S}(x) &= 2iN_0\pi T \sum_{\omega_m>0} f_s \boldsymbol{f}_t(x) \\ &= \sum_{n=1,2} \chi(x, x_n) G_n \boldsymbol{m}_n.\end{aligned} \tag{4}$$

On the second line, we define the nonlocal spin susceptibility $\chi(x, x')$.

Substituting Eq. (3b) into Eq. (2), we find the SS

$$j_{xx}^{\mathrm{eq}} = G_1 G_2 \chi(x_1, x_2) \sin\phi. \tag{5}$$

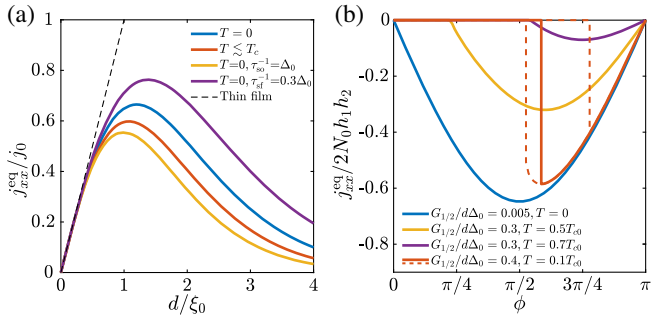

FIG. 2. (a) Spin supercurrent as a function of SC thickness with fixed $h_n \ll \Delta_0$ normalized by $j_0 = h_1 h_2 \sin\phi \lim_{d\to 0}[\chi(x_1, x_2)d]\xi_0$. (b) Spin current-magnetization angle relation for $d = \xi_0$ with no spin scattering. Dashed lines indicate SC-N state hysteresis.

In analogy to the SNS junction, the FSF trilayer can be considered a spin Josephson junction [19,20]. The middle layer is weak in the sense that it cannot support multiple phase windings, since there is no energy penalty for the vanishing condensate function. In order to have strong SS with a total phase winding larger than π would require the condensate to be restricted to U(1) symmetry, as happens, e.g., in easy-plane ferromagnets [1,21]. Figure 2(b) shows the current-angle relation, which deviates from sine function at high T and at strong coupling.

As an equilibrium current, $\boldsymbol{j}_x^{\mathrm{eq}}$ is conserved through the SC [22]. Figure 2(a) shows its magnitude as a function of d. In the thin-film limit $d \ll \xi_0$, where ξ_0 is the SC coherence length, each interface induces a homogeneous exchange field with amplitude $h_n = G_n/d$ [23]. The total exchange field is $\boldsymbol{h} = h_1\boldsymbol{m}_1 + h_2\boldsymbol{m}_2$ is limited by the Chandrasekhar-Clogston critical value $h_c = \Delta_0/\sqrt{2}$. With fixed h_n the SS is proportional to d. When $d \to \infty$, the supercurrent vanishes as $\exp(-d/\xi_0)$. This exponential factor measures the overlap between the two proximity fields. Maximal SS is obtained when the maximum volume of SC is proximitized by both FIs at $d \approx \xi_0$.

Boundary conditions.—At arbitrary temperatures and with finite spin-orbital or spin-flip scattering times $\tau_{\mathrm{so/sf}}$, we determine the SC spin accumulation in the dirty limit from the full Usadel equation [24], using the spin-mixing BC [15,32]

$$D\boldsymbol{n} \cdot \check{g} \circ \nabla \check{g}|_{x=x_n} = iG_n[\boldsymbol{m}_n \cdot \boldsymbol{\sigma}\tau_3 \circ, \check{g}], \tag{6}$$

where $\check{g}$ are the 8×8 quasiclassical Green's functions in Keldysh-Nambu-Spin space and $\circ$ products are time convolutions. The above BC gives Eq. (3b) as a special case. In the BC we take into account only the effective exchange field, [15] and neglect terms associated with interfacial spin relaxation and decoherence [33–35].

By taking the trace over spin of Eq. (6), and integrating over the energy, the spin current through the nth interface is [36]

$$\boldsymbol{j}_{x,n}(t) = G_n[\boldsymbol{S}(t,x_n)\times\boldsymbol{m}_n(t) - N_0\dot{\boldsymbol{m}}_n(t)], \tag{7}$$

where $\boldsymbol{S}$ contains both the equilibrium spin density cf. Eq. (4) and the nonequilibrium spin accumulation within the SC. We assume that $d \gg \lambda_F$, where λ_F is the Fermi wavelength, and neglect the short range Pauli paramagnetic contribution. The $\dot{\boldsymbol{m}}_n$ term is the spin pumping contribution, and $\boldsymbol{S}\times\boldsymbol{m}_n$ gives the equilibrium SS and the back-action due to nonequilibrium spin accumulation induced by spin pumping [37]. According to Eq. (7) there is a finite SS if the equilibrium $\boldsymbol{S}$ and the magnetization of the FI are not collinear.

Magnetic hysteresis.—We introduce a Stoner-Wohlfarth type free energy (per interface area) to describe the effect of SS on the magnetic configuration of the FI/SC/FI trilayer [38]

$$F(\boldsymbol{m}_1,\boldsymbol{m}_2) = \sum_{n=1,2}[-\mu_0\boldsymbol{M}_n\cdot\boldsymbol{H} - K_A^n(\boldsymbol{m}_n\cdot\boldsymbol{z})^2 + K_B^n(\boldsymbol{m}_n\cdot\boldsymbol{x})^2] + F_{\rm sc}(\boldsymbol{m}_1\cdot\boldsymbol{m}_2,\Delta), \tag{8}$$

where $|\boldsymbol{M}_n| = M_n$ is the FI magnetic moment per interface area. The free energy includes the Zeeman energy from external magnetic field $\boldsymbol{H}$, the SC free energy $F_{\rm sc}$, and the in-plane easy axis or out-of-plane anisotropy energies $K_{A/B}^n$. In the thin-film limit, at $T=0$ and without any spin scattering $F_{\rm sc}(\boldsymbol{h}) = dN_0(|\boldsymbol{h}|^2 - \Delta^2/2)$. In the general case we use the SC energy functional of Ref. [39].

In a static setting, the coupling between the magnets can be described as an effective magnetic field $\mu_0\boldsymbol{H}_{\rm eff,1}^{\rm sc} = -J_\phi\boldsymbol{m}_2/M_1$, which can be identified with SS via the spin-transfer torque

$$\boldsymbol{j}_{x,1}^{\rm eq} = -\boldsymbol{M}_1\times\mu_0\boldsymbol{H}_{\rm eff,1}^{\rm sc} = J_\phi\boldsymbol{m}_1\times\boldsymbol{m}_2, \tag{9}$$

with exchange constant $J_\phi = dF_{\rm sc}/d\cos\phi \geq 0$. At weak coupling Eq. (9) coincides with Eq. (5).

When the SC exchange energy is small compared to the anisotropy energies, SS modifies the coercive fields [40] [Fig. 3(a)]. In the SC state, the coercive fields for AP-to-P switching increase by J_π/M_n, and the coercive fields for P-to-AP switching decrease by J_0/M_n relative to the N state. With a strong SS [Fig. 3(b)] the anisotropies cannot force the magnets into a binary parallel or antiparallel configuration space and the exchange interaction may induce a spin-flop transition, in which the two magnets collectively rotate from the AP to P configuration [41].

At low temperatures the SC transition is of the first order as a function of ϕ and exhibits hysteresis [Fig. 2(b)] [25,26,42,43]. If there is a strong uniaxial anisotropy in the FIs, it is possible to study the N-to-SC hysteresis [42,43], as opposed to the ordinary magnetic hysteresis resulting from anisotropies. By applying the external magnetic field perpendicular to the easy-axis direction, the exchange field changes continuously. If the SC transition is continuous, there is also no magnetic hysteresis. If the transition is of the first order, the N-to-SC and magnetic hysteresis become entangled. We show in the Supplemental Material how the two can be disentangled in the magnetization curve [24].

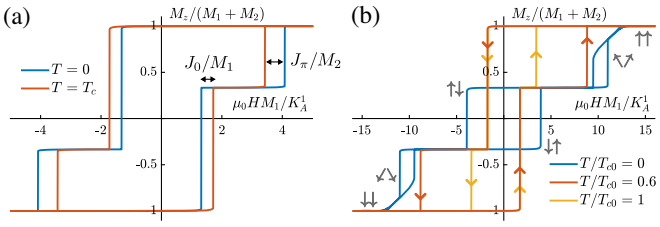

FIG. 3. Hysteresis loops for two coupled ferromagnets. (a) Weak SC exchange interaction $dN_0\Delta_0^2/K_A^n = 1$. For $T=0$ the system is always in the SC state. (b) Strong exchange interaction $dN_0\Delta_0^2/K_A^n = 15$. For $T/T_c = 0.6$ the system is in the N state in the P configuration, but in the SC state for the AP configuration. For both panels, $M_1 = 2M_2$, $h_n = 0.3\Delta_0$, and $\tau_{\rm so/sf}^{-1} = 0$. External field is at 2° angle to the anisotropy axis.

Magnetization dynamics.—We now consider the dynamical effects due to SS. In contrast to most studies of F/SC hybrid structures [44,45], we take both magnets as dynamical. We study the small-angle dynamics around the equilibrium configuration with the ansatz

$$\boldsymbol{m}_n(t) = \boldsymbol{m}_n(0) + \Re[\boldsymbol{m}_n(\omega)\exp(-i\omega t)], \tag{10}$$

where $\boldsymbol{m}_n(\omega)$ is a small perturbation perpendicular to $\boldsymbol{m}_n(0)$. The dynamical magnetization induces a time-dependent exchange field at the SC interfaces, which in turn induces a time-dependent spin density in the SC.

The dynamics of the FI magnetizations are described by the classical Landau-Lifshitz-Gilbert (LLG) equation, supplemented by a spin current term [46]

$$\dot{\boldsymbol{M}}_n = -\gamma\boldsymbol{M}_n\times\mu_0\boldsymbol{H}_{\rm eff,n}^{(0)} + \frac{\alpha_n}{M_n}(\boldsymbol{M}_n\times\dot{\boldsymbol{M}}_n) + \gamma\boldsymbol{j}_{x,n}, \tag{11}$$

where $\boldsymbol{H}_{\rm eff,n}^{(0)}$ is the effective magnetic field in the N state including the external magnetic field and anisotropy fields, γ is the gyromagnetic ratio, and α_n is the Gilbert damping coefficient, which can be controlled with an additional heavy metal layer next to the FI [Fig. 1(b)]. The spin current is given by Eq. (7).

In a FMR experiment, the external field has a static component and a small transverse dynamic part $\boldsymbol{H}_{\rm rf}$. The linear response to $\boldsymbol{H}_{\rm rf}$ given by LLG Eq. (11) is

$$\hat{\chi}_n^{-1}(\omega)\boldsymbol{M}_n(\omega) = \mu_0\boldsymbol{H}_{\rm rf}(\omega) - \boldsymbol{m}_n(0)\times\frac{\boldsymbol{j}_{x,n}(\omega)}{M_n}, \tag{12}$$

where $\hat{\chi}_n^{-1}$ are the 2×2 magnetic susceptibilities of the uncoupled magnets [24]. As the magnets are insulating, they support no eddy currents, and the layers do not couple inductively [47,48]. We also assume that the lateral size of the films is much larger than their thickness, and neglect the magnetostatic coupling between the layers.

In the parallel configuration, the coupled dynamics of the two magnets is described by a matrix susceptibility

$$\hat{\chi}_{\rm tot}^{-1}(\omega)=\begin{pmatrix}\hat{\chi}_1^{-1}(\omega)+\frac{J_0-\delta\hat{J}_{11}(\omega)}{M_1^2} & -\frac{J_0+\delta\hat{J}_{12}(\omega)}{M_1M_2}\\ -\frac{J_0+\delta\hat{J}_{21}(\omega)}{M_1M_2} & \hat{\chi}_2^{-1}(\omega)+\frac{J_0-\delta\hat{J}_{22}(\omega)}{M_2^2}\end{pmatrix}, \quad (13)$$

where $J_0=-G_1G_2\chi(x_1,x_2)$ is the static exchange constant, and

$$\delta\hat{J}_{ij}(\omega)=-G_iG_j[\hat{\chi}(\omega,x_i,x_j)-\chi(x_i,x_j)]-N_0G_i\omega\delta_{ij}\hat{\sigma}_3, \quad (14)$$

are the dynamic corrections related to spin pumping and other finite-frequency processes. Here, $\hat{\chi}$ is the dynamic spin susceptibility [24,49], related to the static spin susceptibility by $\hat{\chi}(0,x_i,x_j)=\chi(x_i,x_j)\hat{1}$.

To illustrate the effect of SS on the FMR properties, we first consider a fully symmetric trilayer. In the P configuration, the eigenmodes are the acoustic and optical modes for which $\boldsymbol{m}_1(t)=\pm\boldsymbol{m}_2(t)$, respectively [41]. In the acoustic mode, the magnetizations are always parallel to each other and there is no SS [41]. The magnets are only coupled by the residual part of the susceptibility, $\chi(\omega)-\chi(0)\approx\omega\chi'(0)$. The imaginary part $\Im\chi'(0)$ contributes directly to dissipation and can be included in the Gilbert damping coefficient. It describes the relaxation of quasiparticles, and vanishes at low T where quasiparticles cannot be excited due to the SC gap [50]. This leads to the usual decrease of the FMR linewidth in the SC state [Fig. 4(a)]. The real part $\Re\chi'(0)$ shifts the resonance frequency.

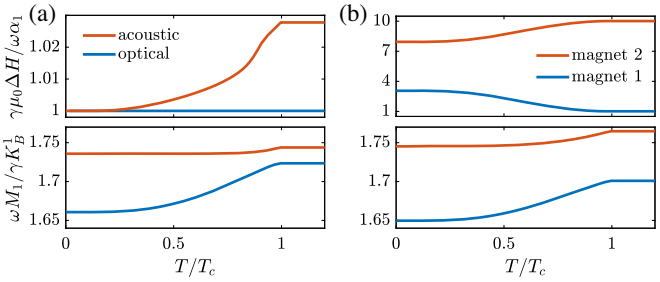

FIG. 4. Temperature dependence of linewidth (top) and resonance frequency (bottom) for (a) a symmetric system with $\alpha_n=0.005$, (b) asymmetric system with $\alpha_1=0.005$ and $\alpha_2=0.05$. Parameters: $K_A^n=0$, $dN_0\Delta_0^2=0.1$, $\Delta_0M_n/\gamma=100$, and $\gamma\mu_0M_nH=1$, in units of K_B^n; $h_n=0.3\Delta_0$, $\tau_{\rm so}^{-1}=0.2\Delta_0$.

In the optical mode the magnetizations precess out of phase and are strongly coupled by the SS. In this case, the effective magnetic field is shifted by $2J_0/M_n$. The resonance field difference between acoustic and optical modes at fixed frequency gives a direct measure of SS. However, measuring the optical mode can be difficult as a symmetrically applied rf field excites only the acoustic mode. The optical mode can be excited by longitudinal FMR pumping [51,52], or by breaking the symmetry. For the optical mode the nonequilibrium spin currents pumped by the two magnets partially cancel in the SC spacer. In the thin-film limit this cancellation is exact and the dissipation in the spacer does not affect the linewidth.

In an asymmetric trilayer, SS can have a drastic effect on the linewidths of the FMR modes. For illustration, let us neglect the spin pumping and consider only the effect of SS together with the intrinsic damping of the magnets. In the N state the magnets are uncoupled, and the eigenmodes are the Kittel modes of the individual magnets with linewidths ΔH_n^0 proportional to Gilbert damping constants α_n. In the SC state, the SS hybridizes the modes so that their linewidths become weighted averages $\Delta H_n=(\Delta H_1^0+p_n\Delta H_2^0)/(1+p_n)$, where $p_1=0$ and $p_2=\infty$ in the uncoupled system, and $p_1\to M_1/M_2$ and $p_2\to M_2/M_1$ in the strongly coupled system [53]. The top panel of Fig. 4(b) shows a numerical evaluation for the linewidth of such a system, including the spin pumping contribution. In particular, if one magnet has a lower intrinsic damping than the other magnet, the linewidth of the related mode increases below the SC transition.

The SS-mediated exchange interaction and spin pumping depend on temperature in opposite ways; spin pumping vanishes at zero temperature, whereas SS vanishes in the normal state. The competition between these two processes can be studied at a mode crossing between two FMR modes (Fig. 5), which can be engineered, e.g., by having FI films with different thicknesses. In general, thinner films will have stronger anisotropy fields. A mode crossing may then be seen by rotating the applied in-plane magnetic field relative to the anisotropy axis [54].

In the N state [Fig. 5(a)] the magnets are only coupled by spin pumping. The dissipative component of spin pumping generated by spin relaxation in the SC layer gives rise to mode attraction. Its signature is the sudden change of the mode linewidths at the mode crossing [inset of Fig 5(a)] [37,55]. In the SC state [Fig. 5(b)], the SS mediated exchange coupling dominates over spin pumping, creating a regular avoided crossing.

So far the dynamical properties of SS have been experimentally studied only in systems with ferromagnetic metals (FM) [2–4], and an increase in FMR linewidth below T_c has been observed in systems which include multiple FM or heavy metal layers with strong spin-orbit coupling. In some of these experiments [2], there is nominally only a single magnet, but the heavy metal layers

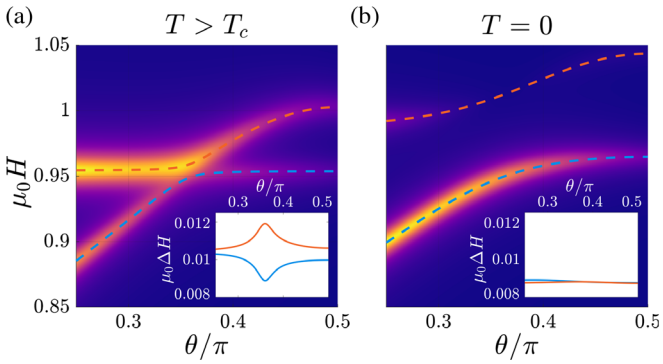

FIG. 5. Absorbed rf power as a function of external field angle θ and amplitude $\mu_0 H$ (in units of K_B^1/M_1). Dashed lines indicate the resonance fields and the insets show the linewidths. (a) Mode locking in the N state is the most evident from the linewidth broadening or narrowing near the crossing. (b) Avoided crossing in the SC state. The linewidths do not depend strongly on the proximity to the crossing. Parameters are as in Fig. 4(a) except for $\omega M_1/\gamma = 1.75$, $K_A^1 = 0.1$, $K_B^2 = 1.1$, and $\Delta_0 M_n/\gamma = 10$, given in units of K_B^1.

close to the ferromagnetic instability can be magnetized by the SS-mediated magnetic proximity effect [56].

With minor changes, our theory can describe SS-mediated coupling in the FM-SC-FM trilayer. The form of the magnetic susceptibility (13) is otherwise unchanged from the insulating case, but the susceptibilities for the spin density at the interfaces are replaced by the susceptibilities for the total spin density of the FM conduction electrons, and the spin mixing conductance is replaced by the s-d coupling inside the FM. In contrast to an FI, in FM the spin current is not absorbed in a layer of atomic thickness, but penetrates into the FM at the range of $\xi_F = \sqrt{D_F/2T}$, where D_F is the diffusion coefficient of the FM [12]. The long-range triplet component [12] penetrating deep into the FM is exactly the component noncollinear to its exchange field, and the one related to SS. Because FMs support eddy currents, there is also an electromagnetic coupling between the layers [47,48]. Finding the magnitude of spin currents in a metallic system will be left for further work.

Despite these differences, our framework suggests that the experimentally observed enhancement below T_c is likely to be a result of SS-mediated hybridization between the FMR modes. In interpreting the FMR data in systems with superconducting interlayers and multiple magnets, one should not rely on the spin pumping picture with a single dynamical magnet, but instead model the magnetization dynamics of the whole structure.

We have studied the properties of SS in FI-SC-FI systems and shown how they can mediate damping between ferromagnetic insulators even though they, as equilibrium currents, are themselves nondissipative. In an analogy to Josephson junctions, the SS can be characterized via the spin current—magnetization angle relation. This can be accessed by studying temperature dependent modifications to the FMR frequencies in FI-SC-FI setups.

The phenomena described here can be studied in various different FI-SC combinations, provided they can be suitably stacked or placed next to each other. The FI can be, for example, GdN, EuS/EuO, or ferrimagnetic YIG, which have been recently studied in combination with superconductors such as Nb, NbN, or Al [40,57–62]. Our results can be used to design magnetic resonator structures where the SS mediates a tunable coupling between the resonators.

This work was supported by the Academy of Finland Projects 297439 and 317118, the European Union's Horizon 2020 Research and Innovation Framework Programme under Grant No. 800923 (SUPERTED), and Jenny and Antti Wihuri Foundation. F. S. B. acknowledges funding by the Spanish Ministerio de Ciencia e Innovacion (MICINN) through Projects FIS2017-82804-P and PID2020-114252GB-I00 (SPIRIT).

[1] E. Sonin, Adv. Phys. **59**, 181 (2010).
[2] K.-R. Jeon, C. Ciccarelli, A. J. Ferguson, H. Kurebayashi, L. F. Cohen, X. Montiel, M. Eschrig, J. W. A. Robinson, and M. G. Blamire, Nat. Mater. **17**, 499 (2018).
[3] K.-R. Jeon, C. Ciccarelli, H. Kurebayashi, L. F. Cohen, X. Montiel, M. Eschrig, S. Komori, J. W. A. Robinson, and M. G. Blamire, Phys. Rev. B **99**, 024507 (2019).
[4] K.-R. Jeon, X. Montiel, S. Komori, C. Ciccarelli, J. Haigh, H. Kurebayashi, L. F. Cohen, A. K. Chan, K. D. Stenning, C.-M. Lee, M. Eschrig, M. G. Blamire, and J. W. A. Robinson, Phys. Rev. X **10**, 031020 (2020).
[5] S. H. Jacobsen, I. Kulagina, and J. Linder, Sci. Rep. **6**, 23926 (2016).
[6] F. Aikebaier, M. A. Silaev, and T. T. Heikkilä, Phys. Rev. B **98**, 024516 (2018).
[7] M. Büttiker, Y. Imry, and R. Landauer, Phys. Lett. **96A**, 365 (1983).
[8] L. P. Lévy, G. Dolan, J. Dunsmuir, and H. Bouchiat, Phys. Rev. Lett. **64**, 2074 (1990).
[9] A. Bleszynski-Jayich, W. Shanks, B. Peaudecerf, E. Ginossar, F. von Oppen, L. Glazman, and J. Harris, Science **326**, 272 (2009).
[10] P.-G. de Gennes, Phys. Lett. **23**, 10 (1966).
[11] F. S. Bergeret, A. F. Volkov, and K. B. Efetov, Phys. Rev. Lett. **86**, 4096 (2001).
[12] F. S. Bergeret, A. F. Volkov, and K. B. Efetov, Rev. Mod. Phys. **77**, 1321 (2005).
[13] J. Linder and A. V. Balatsky, Rev. Mod. Phys. **91**, 045005 (2019).
[14] J. A. Ouassou, J. W. Robinson, and J. Linder, Sci. Rep. **9**, 12731 (2019).
[15] T. Tokuyasu, J. A. Sauls, and D. Rainer, Phys. Rev. B **38**, 8823 (1988).
[16] D. Huertas-Hernando, Y. V. Nazarov, and W. Belzig, Phys. Rev. Lett. **88**, 047003 (2002).
[17] F. S. Bergeret, A. F. Volkov, and K. B. Efetov, Phys. Rev. B **69**, 174504 (2004).

[18] J. Xia, V. Shelukhin, M. Karpovski, A. Kapitulnik, and A. Palevski, Phys. Rev. Lett. **102**, 087004 (2009).
[19] I. Fomin, Physica (Amsterdam) **169B**, 153 (1991).
[20] F. S. Nogueira and K.-H. Bennemann, Europhys. Lett. **67**, 620 (2004).
[21] S. Takei and Y. Tserkovnyak, Phys. Rev. Lett. **112**, 227201 (2014).
[22] J. A. Ouassou, A. Pal, M. Blamire, M. Eschrig, and J. Linder, Sci. Rep. **7**, 1932 (2017).
[23] T. T. Heikkilä, M. Silaev, P. Virtanen, and F. S. Bergeret, Prog. Surf. Sci. **94**, 100540 (2019).
[24] See Supplemental Material at http://link.aps.org/supplemental/10.1103/PhysRevLett.128.167701, which includes derivations for the thin-film spin susceptibility and the coupled magnetic susceptibility, including Refs. [25–31]. Codes are available at gitlab.jyu.fi/jyucmt/fi-sc-fi.
[25] K. Maki and T. Tsuneto, Prog. Theor. Phys. **31**, 945 (1964).
[26] P. Tedrow, R. Meservey, and B. Schwartz, Phys. Rev. Lett. **24**, 1004 (1970).
[27] F. Aikebaier, P. Virtanen, and T. Heikkilä, Phys. Rev. B **99**, 104504 (2019).
[28] K. D. Usadel, Phys. Rev. B **4**, 99 (1971).
[29] M. Eschrig, Phys. Rev. B **61**, 9061 (2000).
[30] K. Yosida, Phys. Rev. **110**, 769 (1958).
[31] A. A. Abrikosov and L. P. Gor'kov, Zh. Eksp. Teor. Fiz. **42**, 1088 (1962) [Sov. Phys. JETP **15**, 752 (1962)].
[32] M. A. Silaev, R. Ojajärvi, and T. T. Heikkilä, Phys. Rev. Research **2**, 033416 (2020).
[33] F. S. Bergeret, A. Verso, and A. F. Volkov, Phys. Rev. B **86**, 214516 (2012).
[34] M. Eschrig, A. Cottet, W. Belzig, and J. Linder, New J. Phys. **17**, 083037 (2015).
[35] X.-P. Zhang, F. S. Bergeret, and V. N. Golovach, Nano Lett. **19**, 6330 (2019).
[36] R. Ojajärvi, T. T. Heikkilä, P. Virtanen, and M. A. Silaev, Phys. Rev. B **103**, 224524 (2021).
[37] Y. Tserkovnyak, A. Brataas, G. E. W. Bauer, and B. I. Halperin, Rev. Mod. Phys. **77**, 1375 (2005).
[38] E. C. Stoner and E. Wohlfarth, Phil. Trans. R. Soc. A **240**, 599 (1948).
[39] P. Virtanen, A. Vargunin, and M. Silaev, Phys. Rev. B **101**, 094507 (2020).
[40] Y. Zhu, A. Pal, M. G. Blamire, and Z. H. Barber, Nat. Mater. **16**, 195 (2017).
[41] P. Wigen, Z. Zhang, L. Zhou, M. Ye, and J. Cowen, J. Appl. Phys. **73**, 6338 (1993).
[42] W. Wu and P. W. Adams, Phys. Rev. Lett. **74**, 610 (1995).
[43] V. Y. Butko, P. W. Adams, and E. I. Meletis, Phys. Rev. Lett. **83**, 3725 (1999).
[44] H. T. Simensen, L. G. Johnsen, J. Linder, and A. Brataas, Phys. Rev. B **103**, 024524 (2021).
[45] X. Montiel and M. Eschrig, arXiv:2106.13988.
[46] J. C. Slonczewski, J. Magn. Magn. Mater. **159**, L1 (1996).
[47] M. Müller, L. Liensberger, L. Flacke, H. Huebl, A. Kamra, W. Belzig, R. Gross, M. Weiler, and M. Althammer, Phys. Rev. Lett. **126**, 087201 (2021).
[48] K. Kennewell, M. Kostylev, and R. Stamps, J. Appl. Phys. **101**, 09D107 (2007).
[49] M. A. Silaev, Phys. Rev. B **102**, 144521 (2020).
[50] J. P. Morten, A. Brataas, G. E. W. Bauer, W. Belzig, and Y. Tserkovnyak, Europhys. Lett. **84**, 57008 (2008).
[51] Z. Zhang, L. Zhou, P. E. Wigen, and K. Ounadjela, Phys. Rev. Lett. **73**, 336 (1994).
[52] J. Lindner and K. Baberschke, J. Phys. Condens. Matter **15**, R193 (2003).
[53] A. Layadi, AIP Adv. **5**, 057113 (2015).
[54] B. Heinrich, Y. Tserkovnyak, G. Woltersdorf, A. Brataas, R. Urban, and G. E. W. Bauer, Phys. Rev. Lett. **90**, 187601 (2003).
[55] Y. Tserkovnyak, Phys. Rev. Research **2**, 013031 (2020).
[56] X. Montiel and M. Eschrig, Phys. Rev. B **98**, 104513 (2018).
[57] Y. Yao, Q. Song, Y. Takamura, J. P. Cascales, W. Yuan, Y. Ma, Y. Yun, X. C. Xie, J. S. Moodera, and W. Han, Phys. Rev. B **97**, 224414 (2018).
[58] A. Hijano, S. Ilić, M. Rouco, C. González-Orellana, M. Ilyn, C. Rogero, P. Virtanen, T. T. Heikkilä, S. Khorshidian, M. Spies, N. Ligato, F. Giazotto, E. Strambini, and F. S. Bergeret, Phys. Rev. Research **3**, 023131 (2021).
[59] B. Li, N. Roschewsky, B. A. Assaf, M. Eich, M. Epstein-Martin, D. Heiman, M. Münzenberg, and J. S. Moodera, Phys. Rev. Lett. **110**, 097001 (2013).
[60] J. P. Cascales, Y. Takamura, G. M. Stephen, D. Heiman, F. S. Bergeret, and J. S. Moodera, Appl. Phys. Lett. **114**, 022601 (2019).
[61] E. Strambini, V. N. Golovach, G. De Simoni, J. S. Moodera, F. S. Bergeret, and F. Giazotto, Phys. Rev. Mater. **1**, 054402 (2017).
[62] K. Rogdakis, A. Sud, M. Amado, C. M. Lee, L. McKenzie-Sell, K. R. Jeon, M. Cubukcu, M. G. Blamire, J. W. A. Robinson, L. F. Cohen, and H. Kurebayashi, Phys. Rev. Mater. **3**, 014406 (2019).